CML 90-3

A Constitutive Model for AS4/PEEK Thermoplastic Composites Under Cyclic Loading

Yuting Rui and C. T. Sun
School of Aeronautics and Astronautics
Purdue University
West Lafayette, IN 47907

October 1990

A technical report submitted to

NASA Langley Research Center

Hampton, Virginia

Abstract

Based on the basic and essential features of the elastic-plastic response of the AS4/PEEK thermoplastic composite subjected to off-axis cyclic loadings, a simple rate-independent constitutive model is proposed to describe the orthotropic material behavior for cyclic loadings. A one-parameter memory surface is introduced to distinguish the "virgin" deformation and the subsequent deformation process and to characterize the loading range effect. Cyclic softening is characterized by the change of generalized plastic modulus. By the vanishing yield surface assumption, a yield criterion is not needed and it is not necessary to consider loading and unloading separately. The model is compared with experimental results and good agreement is obtained.

1. Introduction

AS4/PEEK thermoplastic composite contains AS4 graphite fibers and thermoplastic matrix PEEK (polyether ether ketone). Compared with other types of thermoplastic matrix, PEEK has higher ductility, higher operating temperature and is unaffected by solvents. Due to the higher ductility of the matrix, AS4/PEEK exhibits pronounced plasticity even at low stress levels. Therefore, it is important to describe the plastic behavior of the composite. The study of cyclic plasticity of the composite material is further motivated by applications in engineering structures subjected to cyclic loads, or to cycles of temperature, which result in cyclic inelastic responses and fatigue failure.

Isotropic hardening, which assumes that a yield surface expands isotropically during plastic flow, gives good results for simple loading but contradicts the Bauschinger effect. Kinematic hardening, one of most important concepts to account for loading history associated with change of loading direction, was introduced by Ishlinskii [1] and Prager [2], and was improved by Zieglar [3]. According to the kinematic hardening rule, the yield surface does not change its initial form and orientation but translates in the stress space like a rigid body. A more complex work-hardening model introducing deformation and rotation of yield surface was introduced by Baltov and Sawczuk [4]. Phillips et al [5,6] proposed a model introducing the anisotropic hardening and cross-hardening effects of the yield surface.

In the above models, emphasis was placed on how to describe the change of the yield surface during plastic deformation little has been done as to how the work hardening plastic modulus changes, which is essential to complex loading histories, such as cyclic loading history. To describe the change of the work hardening plastic modulus, Eisenberg and Phillips [7] generalized the bilinear approximation model proposed by Prager [8] to include nonlinear hardening materials. They used accumulated plastic deformation in uniaxial reverse loading to

obtain a description of the material, which predicts the same value of plastic modulus at the termination of plastic loading as that at the beginning of the reversed plastic loading. In order to describe the transient stress-strain behavior, which is usually characterized by cyclic hardening or softening, Eisenberg and Yen [9] demonstrated that the Ramberg-Osgood parameters (k, n) may be considered to be cycle-dependent. Dafalias and Popov [10] and Krieg [11] introduced the concept of a bounding surface in the stress space which always encloses the loading surface. A parameter defined by the relative position of the loading and the bounding surface and the plastic work done during the most recent loading determines the value of the plastic modulus.

In a different approach, Mroz [12] introduced the concept of a "field of work hardening moduli". This field is defined by a configuration of surfaces of constant work hardening moduli in the stress space. A stable cyclic stress-strain curve for Masing type material is determined by calculation of the translation of surfaces. Hardening or softening behavior is achieved by permitting one or more nested surface to expand or contract. He also proposed a new rule of kinematic hardening which is different from those of Prager and Ziegler. In the multi-surface approach, more models using two or more surfaces have been proposed by McDowell [13], Tseng and Lee [14], Hashiguchi [15].

A few attempts have been made for the determination of inelastic-behavior of metal-matrix composite for cyclic loading. Dvorak and Bahei-El-Din [16] proposed a micromechanical model in which the elastic-plastic behavior of composite is described in terms of the constituent properties, their volume fractions, and material constraints between the phases. The matrix was assumed to be the Mises-type and to obey the Prager-Ziegler kinematic hardening rule. Dvorak and Bahei-El-Din [17] also proposed a bimodal plasticity theory of fibrous composite materials. According to this theory, the overall yield surface of composite is determined by two distinct modes: the matrix-dominated mode and fiber-dominated mode.

Aboudi [18] derived an effective constitutive equation based on a high order continuum theory with microstructure for the modeling of visco-plastic composite. The theory is independent of yield criterion, loading and unloading conditions. The constitutive relations for a single phase constituent are based on a generalization of Prandtl-Reuss flow rule. In the evolution equation for the inelastic state variables that control plastic flow, it is assumed that part of the rate of change is isotropic and remaining part varies according to the sign and orientation of the current rate of deformation vector. This leads to a minimum of twelve components of the internal state tensor which represents resistance to inelastic deformation.

As noted by Bahei-El-Din & Dvorak [19] and Johnson [20], The difficulties encountered in formulating micromechanical models lie in the facts that the in-situ constituent matrix properties are different from those of the bulk matrix material and that 3-D elastic constants of the fiber are difficult to measure. In the above studies [16-19], no experimental results for cyclic loading are available for comparison and verification.

The present study aimed at experimental determination and theoretical modeling of inelastic behavior of AS4/PEEK thermoplastic composite under cyclic loading. A series of tests of cyclic loading on off-axis AS4/PEEK thermoplastic composite specimens were performed. A simple rate-independent constitutive model was developed. Some basic features in this model are: yield surface is one-parameter type; deformation process is decomposed into virgin deformation, which corresponds to initial loading and overloading, and non-virgin deformation, which corresponds to subsequent loading within the previous maximum stress range which is defined by a one-parameter type memory surface. Cyclic softening is achieved by the change of generalized plastic modulus during plastic deformation. For further simplification, the vanishing yield surface assumption was adopted. Good agreement between the experimental results and model simulations was found.

2. Experiment

2.1. Experiment Procedure

The 15°, 30°, 45° and 90° off-axis coupon specimens were cut from the 10-plied unidirectional composite panel of which the thickness was 1.27±0.03 mm. The specimen length was 228 mm, and the width was 25.4 mm. Flexible end tabs made of Flex Epoxy 103 and fiber-glass knit were used to reduce the end effect due to extension-shear coupling [22].

To prevent the specimen from buckling under compression, an antibuckling apparatus was designed and used in the cyclic loading tests. The apparatus shown in Fig. 1 was employed for compression test of off-axis specimens in [23]. It has the following properties:

- It allows the specimen to have a long effective specimen length in order to reduce the end effect due to extension-shear coupling.
- The plane stress state of the specimen should not be affected. For this reason, the lateral pressure on the specimen is kept low enough just to prevent buckling.

The effective specimen length allowed by the apparatus was 152 mm. The specimen was supported by four steel guides. The lateral supporting force was exerted using six springs, and could be adjusted to an appropriate value. In this study, 890 N of supporting force was chosen. The corresponding normal stress due to the supporting force was about 0.23 MPa. In order to minimize the surface friction between the specimen and the steel guides, a thin TX-1040 teflon-coated fabric sheet was put between the specimen and the steel guide. The maximum friction force between the specimen and the steel guide could be reduced to 195 N. The stress caused by the friction force was negligible.

The uniaxial cyclic loading tests were performed using the closed-loop-servo hydraulic MTS 810 machine at room temperature (75°F). All tests were performed at a strain-controlled mode at a constant strain rate $\dot{\varepsilon}_x = 20\ \mu\varepsilon$/sec. Longitudinal and transverse strains were measured by strain gages mounted at the center of the specimen. The measured analog signals were converted into digital signals which were stored and analyzed by an IBM-AT computer data acquisition system.

2.2. Experimental Results

The experimentally determined apparent elastic moduli and Poison's ratios of the off-axis coupon specimens are listed in Table 1. The longitudinal stress-strain curves for the 15°, 30°, 45° and 90° off-axis coupon specimens are shown in Fig. 2-5, respectively.

It can be seen that the material is not Masing-type, and is slightly softened during first few reversals. The stress-strain curves asymptotically approach hysteresis loops. These curves also show that there is no well defined yield point, and the nonlinearity appears gradually, starting near the beginning of the initial curve and of each reversal.

Loading Range Effect: To investigate the effect of loading range (plastic strain range under strain control or load range under stress control) on the material response during reverse loading and subsequent loading, three 30° off-axis specimens were cyclically loaded at strain ranges $\Delta\varepsilon_x$=-0.49/0.49%, -0.69/0.70% and -0.89/0.89% respectively. The longitudinal stress-strain curves are presented in Fig. 6. It can be seen that the shapes of the stress-strain curves are dependent on the loading range, i.e., the larger the loading range, the softer the material behaviors.

One 30° off-axis specimen was cyclicly loaded at $\Delta\varepsilon_x$ = -0.57/0.60% for four cycles first, then cyclicly loaded at $\Delta\varepsilon_x$ = -0.79/0.80%. The stress-strain curves are shown in Fig. 7. It can be seen that additional softening occurs when the loading range increases. For comparison, one 30° off-axis specimen was cyclicly loaded at $\Delta\varepsilon_x$ = -0.79/0.80% for four cycles first, then cyclically loaded at $\Delta\varepsilon_x$ = -0.57/0.60%. The stress-strain curves are plotted in Fig. 8. It can be seen that there is no apparent softening when the loading range is decreased.

3. A Plane Stress Constitutive Model for Cyclic Loading

3.1. Model Description

It has been demonstrated that the plastic properties of unidirectional composites such as boron/aluminum and thermoplastic composites can be well characterized by a one parameter plastic potential function [21-24]. Following a similar approach, we define the yield surface as

$$2f(\sigma_{ij} - \alpha_{ij}) - k^2 = 0 \tag{1}$$

where $f(\sigma_{ij} - \alpha_{ij})$ is a plastic potential function defined by

$$2f(\sigma_{ij} - \alpha_{ij}) = (\sigma_{22}-\alpha_{22})^2 + 2a_{66}(\sigma_{12}-\alpha_{12})^2 \tag{2}$$

in which 1-axis and 2-axis refer to the fiber direction and the transverse direction, respectively, $(\alpha_{22}, \alpha_{12})$ is the center of the yield surface, and k specifies the size of the surface. In the σ_{22} and σ_{12} subspace, equation (1) represents an ellipse. The selection of this yield surface implies that plastic deformation in the fiber direction is absent.

A material is called a virgin material if it has not been loaded or deformed after it is manufactured. The deformation during the initial loading of a virgin material is called virgin deformation. The deformation corresponding to the subsequent loading within the previous maximum stress range is called non-virgin deformation. Once the subsequent loading exceeds the previous maximum stress range (overloading), the deformation is also called virgin deformation.

The maximum stress range is defined by

$$2f(\sigma_{ij}) - q_{max}^2 = 0 \tag{3}$$

where q_{max}^2 is the maximum value of $2f(\sigma_{ij}) = \sigma_{22}^2 + 2a_{66}\sigma_{12}^2$. Henceforth, this surface will be referred to as the memory surface corresponding to loading q_{max}. In the virgin state, the memory surface coincides with the yield surface initially. During initial loading, the memory surface expands isotropically and the yield surface translates. During unloading and subsequent reloading, the yield surface will translate within the memory surface. Once loading reaches the memory surface and exceeds it (overloading), the memory surface will expand again with the loading. Therefore, the virgin deformation corresponds to the expansion of the memory surface, and the non-virgin deformation corresponds to the subsequent loading within the memory surface.

The criterion for virgin deformation is given by

$$2f(\sigma_{ij}) - q_{max}^2 = 0 \quad \text{and} \quad \frac{\partial f(\sigma_{ij})}{\partial \sigma_{ij}} d\sigma_{ij} \geq 0 \tag{4}$$

The reason for distinguishing virgin deformation from non-virgin deformation is that the hardening properties are to be characterized differently with respect to virgin deformation and non-virgin deformation. This distinction was also found to be necessary in some metals

[9–11, 13–14, 25]. A schematic representation of the yield surface and memory surface is shown in Fig. 9.

From Mroz's rule of kinematic hardening [12], the motion of the yield surface is defined in the direction from the current loading point s to the stress point s^{Δ} on the memory surface where the unit outward normal is the same as the unit outward normal to the yield surface at loading point s. In case the yield surface is similar to the memory surface, the mathematical description of the kinematic hardening is given by

$$d\alpha_{ij} = d\sigma_{ij} \tag{5}$$

which guarantees that the yield surface is tangent to the memory surface at the loading point when the yield surface approach the memory surface. Equation (5) also guarantees that the yield surface is tangent to the memory surface at loading point during the expansion of the memory surface.

The total strain increment $d\varepsilon_{ij}$ is decomposed into elastic strain increment $d\varepsilon_{ij}^{e}$ and plastic strain increment $d\varepsilon_{ij}^{p}$ as

$$d\varepsilon_{ij} = d\varepsilon_{ij}^{e} + d\varepsilon_{ij}^{p} \quad , \quad ij = 11,\ 22,\ 12 \tag{6}$$

when $\varepsilon_{12} \equiv \gamma_{12}$ is the engineering shear strain.

By the associated flow rule, the plastic strain increments can be written as

$$d\varepsilon_{ij}^{p} = n_{ij} d\xi \quad , \quad in = 22,\ 12 \tag{7}$$

where n_{ij} is the unit vector normal to the yield surface at loading point, $d\xi = (d\varepsilon_{ij}^{p} d\varepsilon_{ij}^{p})^{\frac{1}{2}}$ is the magnitude of the plastic strain increment which is to be determined from the hardening properties.

Consider the initial loading. Define an effective stress as

$$\bar{\sigma} = \sqrt{3f(\sigma_{ij})} \tag{8}$$

and the corresponding effective plastic strain increment $d\bar{\varepsilon}^p$ as

$$\bar{\sigma} d\bar{\varepsilon}^p = \sigma_{ij} d\varepsilon_{ij}^p \tag{9}$$

Then the effective plastic strain increment can be expressed in terms of plastic strain increments and stress components, i.e..

$$d\bar{\varepsilon}^p = \frac{\sigma_{ij} d\varepsilon_{ij}^p}{\bar{\sigma}} \tag{10}$$

Substitution of (7) into (9) yields

$$d\xi = \frac{\bar{\sigma} d\bar{\sigma}}{H \sigma_{mn} n_{mn}} \qquad mn = 22,\ 12 \tag{11}$$

where $H = d\bar{\sigma}/d\bar{\varepsilon}^p$ is called generalized plastic modulus of the anisotropic material. Substitution of (11) into (7) yields

$$d\varepsilon_{ij}^p = \frac{n_{ij} \bar{\sigma} d\bar{\sigma}}{H \sigma_{mn} n_{mn}} \tag{12}$$

By expressing unit normal n_{ij} explicitly, equation (12) can be further simplified to

$$\begin{Bmatrix} d\varepsilon_{11}^p \\ d\varepsilon_{22}^p \\ d\gamma_{12}^p \end{Bmatrix} = \begin{Bmatrix} 0 \\ \sigma_{22} \\ 2a_{66}\sigma_{12} \end{Bmatrix} \left(\frac{3}{2H}\right)\left(\frac{d\bar{\sigma}}{\bar{\sigma}}\right) \tag{13}$$

The above equation gives the incremental form of stress and plastic strain relations for initial loading. It is assumed that these relations are valid for all virgin deformations.

Now, consider the reverse loading following initial loading. It is obvious that the above effective stress is no longer a proper variable to describe hardening properties. Define an effective stress as

$$\bar{\sigma} = \sqrt{3f(\sigma_{ij} - \sigma^*_{ij})} \tag{14}$$

where σ^*_{ij} are the stresses at the starting yield point s^* of the reverse loading. One may view the stress-strain curve of the reverse loading as the superposition of the deformation during this reverse loading to the stress-strain state at the end of initial loading. Therefore, define an effective plastic strain increment $d\bar{\varepsilon}^p$, such that

$$\bar{\sigma} d\bar{\varepsilon}^p = (\sigma_{ij} - \sigma^*_{ij}) d\varepsilon^p_{ij} \tag{15}$$

The effective plastic strain can be expressed as

$$d\bar{\varepsilon}^p = \frac{(\sigma_{ij} - \sigma^*_{ij}) d\varepsilon^p_{ij}}{\bar{\sigma}^*} \tag{16}$$

Substitution of (7) into (15) yields

$$d\xi = \frac{\bar{\sigma} d\bar{\sigma}}{H(\sigma_{mn} - \sigma^*_{mn}) n_{mn}} \tag{17}$$

where $H = d\bar{\sigma}^* / d\bar{\varepsilon}^p$ is the generalized plastic modulus for reverse loading. Substitution of (17) into (7) yields

$$d\varepsilon^p_{ij} = \frac{n_{ij} \bar{\sigma} d\bar{\sigma}}{H(\sigma_{mn} - \sigma^*_{mn}) n_{mn}} \tag{18}$$

which can be expanded explicitly into

$$\begin{Bmatrix} d\varepsilon_{11}^p \\ d\varepsilon_{22}^p \\ d\gamma_{12}^p \end{Bmatrix} = \begin{Bmatrix} 0 \\ \sigma_{22}-\sigma_{22}^* \\ 2a_{66}(\sigma_{12}-\sigma_{12}^*) \end{Bmatrix} \left(\frac{3}{2H}\right)\left(\frac{d\bar{\sigma}}{\bar{\sigma}}\right) \tag{19}$$

The above equation gives the incremental form of stress and plastic strain relations for reverse loading. It is assumed that these relations are valid for all non-virgin deformations. In that case, σ_{ij}^* represent the stresses at the starting yield point of the current reversal.

3.2. Cyclic Softening Or Hardening

Usually, cyclic softening or cyclic hardening includes the change of yield surface and the change of material resistance to plastic deformation during the course of plastic flow. In the present model, the cyclic softening is achieved by the change of generalized plastic modulus while keeping the shape and size of the yield surface unchanged.

From the experimental results, the material response for non-virgin deformation depends on the loading range and accumulated plastic deformation. Therefore, the generalized plastic modulus for virgin deformation can be expressed as

$$H = H(\bar{\sigma}, q_{max}, \bar{\varepsilon}^p) \tag{20}$$

Taking the generalized plastic modulus for the first reversal as reference, the generalized plastic modulus for second and subsequent reversals is assumed to be of the form

$$H(\bar{\sigma}, \bar{\varepsilon}^p, q_{max}) = H_1(\bar{\sigma}, q_{max})[1 - \alpha(1 - \exp(-\frac{\bar{\varepsilon}^p - \bar{\varepsilon}_1^p}{\omega}))] \tag{21}$$

where $H_1 = H_1(\bar{\sigma}, q_{max})$ is the generalized plastic modulus for first reversal, $\bar{\varepsilon}_1^p$ is the accumulated effective plastic strain at the end of the first reversal, the constant ω determines the softening rate, and the constant α characterizes the magnitude of softening.

The generalized plastic modulus is calibrated by the experimental stress-strain curve of unidirectional off-axis specimen. For off-axis loading, the effective stress can be expressed in terms of applied uniaxial stress σ_x, and the effective plastic strain increment can be expressed in terms of plastic strain increment $d\varepsilon_x^p$. By performing stress transformation and strain transformation, and from (7), (8), (10), (14) and (16), we obtain

for virgin deformation:

$$\begin{aligned} \bar{\sigma} &= h(\theta)\sigma_x \\ d\bar{\varepsilon}^p &= d\varepsilon_x^p / h(\theta) \end{aligned} \tag{22}$$

and for non-virgin deformation:

$$\begin{aligned} \bar{\sigma} &= h(\theta)(\sigma_x - \sigma_x^*) \\ d\bar{\varepsilon}^p &= d\varepsilon_x^p / h(\theta) \end{aligned} \tag{23}$$

where

$$h(\theta) = \left[\frac{3}{2}(\sin^4\theta + 2a_{66}\sin^2\theta\cos^2\theta)\right]^{\frac{1}{2}} \tag{24}$$

The $\bar{\sigma}$ vs. $\bar{\varepsilon}^p$ curve can be plotted for initial loading according to (22), which gives the effective stress-effective plastic strain relation for virgin deformation. this curve should be independent of off-axis angles. The generalized plastic modulus H for virgin deformation simply equals to $H = d\bar{\sigma}/d\bar{\varepsilon}^p = H(\bar{\sigma})$.

The $\bar{\sigma}$ vs. $(\bar{\varepsilon}^p - \bar{\varepsilon}^{p^*})$ curve can be plotted for first reversal according to (23), which gives the effective stress -effective plastic strain relation for first reversal. Here $\bar{\varepsilon}^{p^*}$ is the accumulated effective plastic strain $\bar{\varepsilon}^p$ at the starting yield point of first reversal. This curve should be independent of off-axis angles, but depend on the size of the memory surface q_{max} because of the loading range effect. The generalized plastic modulus H_1 simply equals to $H_1 = d\bar{\sigma}/d\bar{\varepsilon}^p = H_1(\bar{\sigma}, q_{max})$.

3.3. Vanishing Yield Surface Assumption

By examining the stress-strain curve of the AS4/PEEK composite, one can find that there is no well defined yield point on stress-strain curves. Nonlinearity appears gradually and starts near the beginning of the initial loading and each reversal. In view of this, it is of practical interest to assume that the yield surface is vanishingly small. Thus, the yield surface degenerates into a single point which coincides with the stress state. Then the following equations exist

$$\alpha_{ij} = \sigma_{ij} \tag{25}$$

$$d\alpha_{ij} = d\sigma_{ij} \tag{26}$$

The vanishing yield surface is the limiting case when $k \to 0$ in equation (1). The unit vector n_{ij} can be determined by the unit normal on the memory surface at point s^Δ, see Fig. 9. Although the yield surface degenerates to a single point, the unit normal to the memory surface is well defined. Because $d\alpha_{ij} = d\sigma_{ij}$ and from Mroz's rule, the point s^Δ is located as the intersection of the extension of $d\sigma_{ij}$ with the memory surface. It is noted that the location of point s^Δ depends on the kinematic rule assumed. By using the vanishing yield surface assumption, the yield criterion is not needed and it is not necessary to consider loading and unloading separately.

4. Model Verification

The proposed model was applied to simulate the cyclic stress-strain response of the AS4/PEEK thermoplastic composite at room temperature. The parameters used in the model simulations are listed in Table 2.

The value of the anisotropy parameter a_{66} in the plastic potential function was found to be 2.0 for both virgin and nonvirgin deformations. Figure 10 shows the effective stress-effective plastic strain curves obtained from various off-axis specimens for virgin deformation. It is evident that with $a_{66} = 2.0$ these curves collapse into a master curve which can be fitted into the power law $\bar{\varepsilon}^p = 1.8 \times 10^{-9} \bar{\sigma}^{2.8}$ ($\bar{\sigma}$ in MPa). Depending on the strain range of interest, the value of a_{66} can be chosen between 1.5 and 2.0 and still yields reasonably good results [22-23].

Figure 11 shows the effective stress-effective plastic strain curves for the first unloading for the off-axis specimens with the same loading range $q_{max} = 148$ MPa. Again, these curves collapse into a master curve with $a_{66} = 2.0$. This master curve can be fitted by the power law $(\bar{\varepsilon}^p - \bar{\varepsilon}^{p*}) = A\bar{\sigma}^{2.1}$ in which the value of A depends on q_{max}. Using the data for other loading ranges, parameter A is found to be close to a linear function of q_{max} as shown in Fig. 12. Thus, we have

$$A = 0 \ldots q_{max} \tag{27}$$

The simulations of the off-axis cyclic stress-strain curves with the constitutive model thus established are plotted and compared with the experimental results in Fig. 13-18. The agreement between the experimental results and model simulation is good.

5. Conclusions

As a first step toward modeling the cyclic plasticity of laminate composites, the present rate-independent constitutive model is developed for unidirectional composite based on some basic features of the material behaviors. This model has very few material constants and is very simple. All constants or parameters can be determined from simple off-axis cyclic loading tests. The simplicity of this testing procedure makes it attractive for developing similar constitutive models for composites in higher temperature environments.

Acknowledgment

This research was sponsored by NASA lanley Research Center under Grant No. NAG-1-825 with Dr. Catherine A. Bigelow as technical monitor.

References

1. Ishlinskii, A. Iu, "General Theory Of Plasticity With Linear Strain Hardening," *ukr. Mat. Zh.*, Vol. 6, 1954, p. 314.
2. Prager, W., "The Theory Of Plasticity: A Survey Of Recent Achievements," James Clayton Lecture, *Proc. Inst. Mech. Engrs. Lond.*, Vol. 169, 1955, PP 41.
3. Ziegler, H., "A Modification Of Prager's Hardening Rule," *Quarterly of Applied Mathematics, Vol. 17, 1959, pp 55.*
4. Baltov, A., and Sawczuk, A., "A Rule Of Anisotropic Hardening," *Acta Mech.*, Vol. 1, No. 2, pp 81-92.
5. Phillips, Aris and Tang, Jun-ling Tang, "The Effect Of Loading Path On The Yield Surface At Elevated Temperatures," *Int. J. Solids Structures*, Vol. 8, 1972, pp 463-474.
6. Phillips, A. and Weng, G. J., "An Analytical Study Of An Experimentally Verified Hardening Law," *J. Applied Mechanics*, June 1975, pp 75-378.
7. Eisenberg, M. A. and Phillips, A., "On Nonlinear Kinematic Hardening," *Acta Mech.*, Vol. 5, 1968, pp. 1-3.
8. Prager, W., "A New Method Of Analyzing Stresses And Strains In Work Hardening Plastic Solids," *J. of Applied Mechanics*, Vol. 23, 1956, pp 493-496.
9. Eisenberg, M. A. and Yen, C, F., "Application Of A Theory Of Visco-plasticity To Uniaxial Cyclic Loading," *Journal of Engoneering Materials and Technology*, Vol. 105,

April 1983, PP 106-112.

10. Dafalias, Y. F. and Popov, E. P., "A Model Of Nonlinearly Hardening Materials For Complex Loading," *Acta Mechanica 21, 1975, pp. 173-192.*

11. Krieg, R. D., "A Practical Two Surface Plasticity Theory," ASME *J. Applied Mechanics,* Vol. 42, 1975, pp. 641-646.

12. Mroz, Z., "An Attempt To Describe The Behavior Of Metals And Cyclic Loads Using A More General Work-hardening Model," *Acta Mechanica 7,* 1969, pp. 199-212.

13. McDowell, D. C., "A Two Surface Model For Transient Nonproportional Cyclic Plasticity: Part 1. Development Of Appropriate Equations," *Journal of Applied Mechanics,* Vol. 52, June 1985, pp 298-302.

14. Tseng, N. T. and Lee,, G. C., "Simple Plasticity Model Of The Two-surface Type," ASCE *Journal of Engineering Mechanics,* 109, no. 3, 795

15. Hashiguchi, K., "Constitutive Equations Of Elastoplastic Materials With Anisotropic Hardening And Elastic-plastic Transition," *Journal of Applied Mechanics,* Vol. 48, June 1981, pp 297-301.

16. Dvorak, G.J. and Bahei-El-Din, Y.A., "Plasticity Analysis Of Fibrous Composites," *Journal of Applied Mechanics,* Vol. 49, 1982, pp. 327-335.

17. Dvorak, G. J. and Bahei-El-Din, "A Bimodal Plasticity Theory Of Fibrous Composite Materials," *Acta Mechanica 69,* 1987, pp 219-241.

18. Aboudi, J, "Effective Constitutive Equations For Fiber-reinforced Viscoplastic Composites Exhibiting Anisotropic Hardening," *Int. J. Engin Sci.* Vol. 21 No. 9, pp. 1081-1096, 1983.

19. Bahei-El-Din, Y.A. and Dvorak, G.J., "Plastic Deformation Of A Laminated Plate With A Hole," *Journal of Applied Mechanics,* Vol. 47, 1980, pp. 827-832.

20. Johnson, W.S., Lubowinski, S.J., Highsmith, A.L., Brewer, W.D. and Hoogstraten, C.A., "Mechanical Characterization Of SCS6/Ti-15-3 Metal Matrix Composites At Room Temperature," NASP Technical Memorandum 1014, NASA-Langley Research Center, Hampton, Virginia, 1988.

21. Sun, C.T. and Chen, J.L., "A Simple Flow Rule For Characterizing Nonlinear Behavior Of Fiber Composites," *J. Composite Material, 23, 1009.*

22. Sun, C.T. and Yoon, K.J., "Characterization Of Elastic-Plastic Properties Of AS4/APC-2 Thermoplastic Composite," A technical report prepared for NASA Langley Research Center, Hampton, Virginia, August 1988.

23. Sun, C. T. and Rui, Yuting, "Orthotropic Elasto-plastic Behavior Of AS4/APC-2 Thermoplastic Composite In Compression," *Mechanics of Materials,* in press.

24. Sun, C. T. and Chen, J. L., "Mechanical Characterization Of SCS-6/Ti-6-4 Metal Matrix Composite," *Composite Science and Technology,* to appear.

25. Ellyin, F. and Xia Z., "A Rate Independent Constitutive Model For Transient Non-proportional Loading," *J. Mech. Phys. Solids,* Vol. 37, No. 1, pp. 71-91, 1989.

26. Drucker, D. C. and Palgen, L., "On Stress-Strain Relations Suitable For Cyclic And Other Loading," *J. Applied Mechanics,* Vol. 48, September 1981, pp 479-485.

27. Ikegami, K., "A historical Perspective Of Experimental Study On Subsequent Yield Surfaces Of Metals (part I)," *J. of the Society for Material Science (Japan)*, Vol. 24, No. 261, 1975.

28. Ikegami, K., "A Historical Perspective Of Experimental Study On Subsequent Yield Surfaces Of Metals (part II)," *J. of the Society for Material Science (Japan)*, Vol. 24, No. 263, 1975.

Table 1. Apparent elastic moduli and Poisson's ratios of different off-axis specimens at room temperatures.

Angle(Degree)	0 °	15 °	30 °	45 °	90 °
E_x (GPa)	130.8	62.6	25.1	16.9	11.2
ν_{xy}	0.33	0.37	0.36	0.25	0.012

Table 2. Summary of parameters in the model.

Anisotropy parameter:	$a_{66} = 2.0$
$\bar{\sigma}$ vs. $\bar{\epsilon}^p$ curve for virgin deformation:	$\bar{\epsilon}^p = 1.8\text{x}10^{-9}\bar{\sigma}^{2.8}$
$\bar{\sigma}$ vs. $(\bar{\epsilon}^p - \bar{\epsilon}^{p^*})$ curve for first reversal:	$(\bar{\epsilon}^p - \bar{\epsilon}^{p^*}) = A\bar{\sigma}^{2.1}$
	$A = (0.0795\ q_{max} - 7.37)\text{x}10^{-8}$
Cyclic softening parameters:	$\alpha = 0.32, \quad \omega = 0.01$

Units: $\bar{\sigma}$ and q_{max} in MPa.

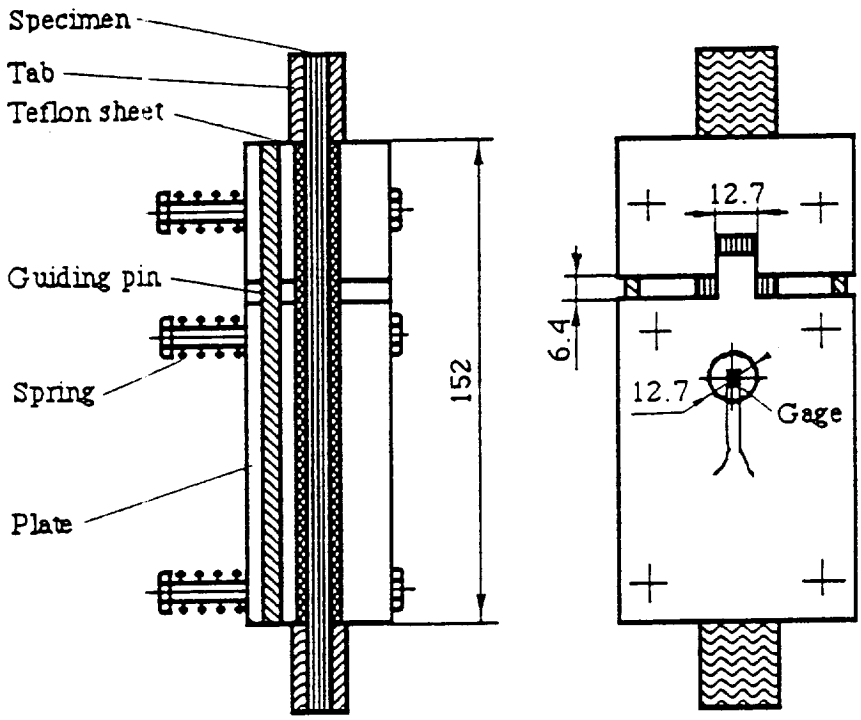

Fig. 1. Schematic of anti-buckling apparatus (unit: mm).

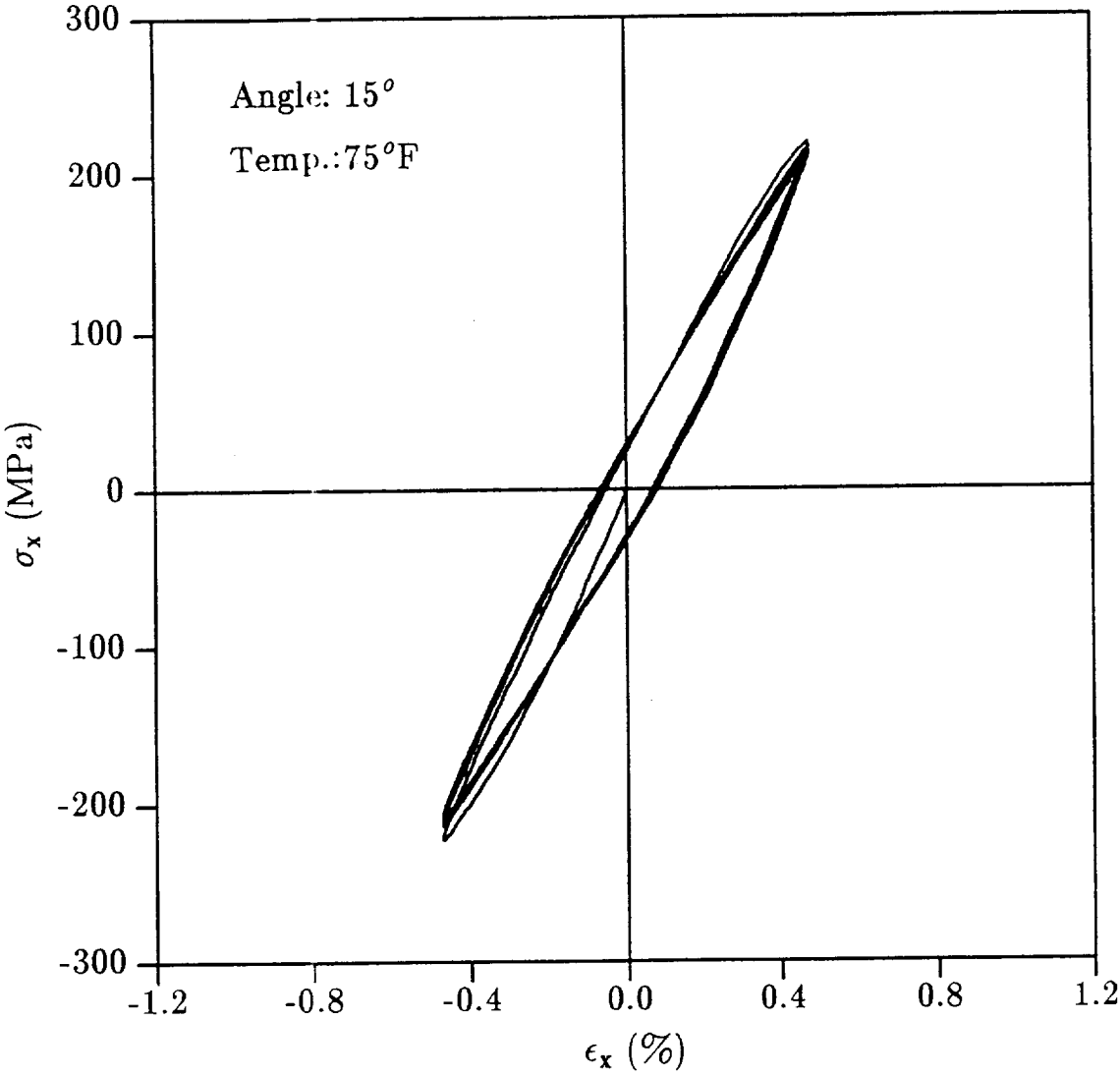

Fig. 2. Stress-strain curve for 15° off-axis specimen of AS4/APC-2 composite at 75°F for first 7 reversals.

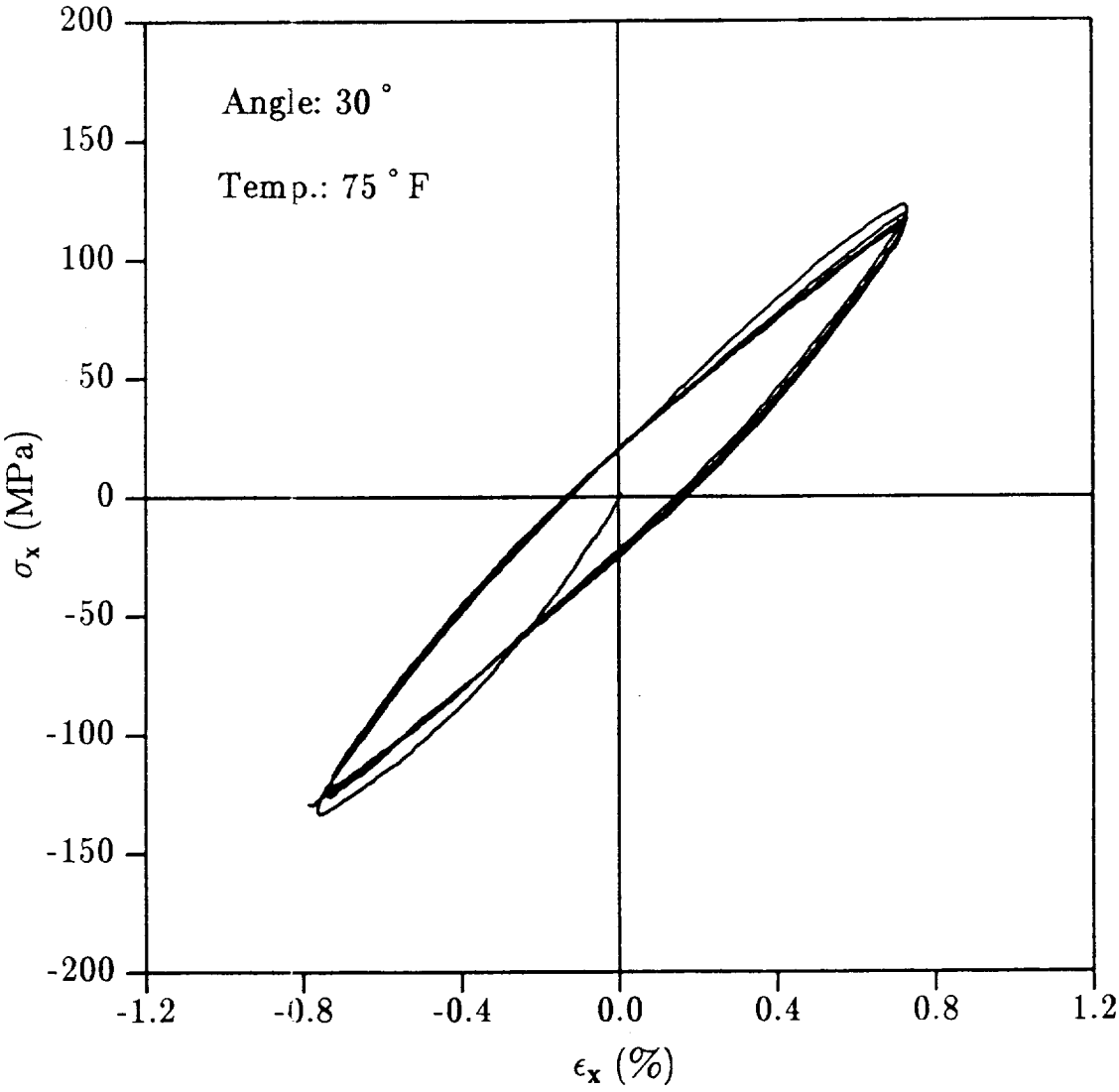

Fig. 3. Stress-strain curve for 30° off-axis specimen of AS4/APC-2 composite at 75°F for first 8 reversals.

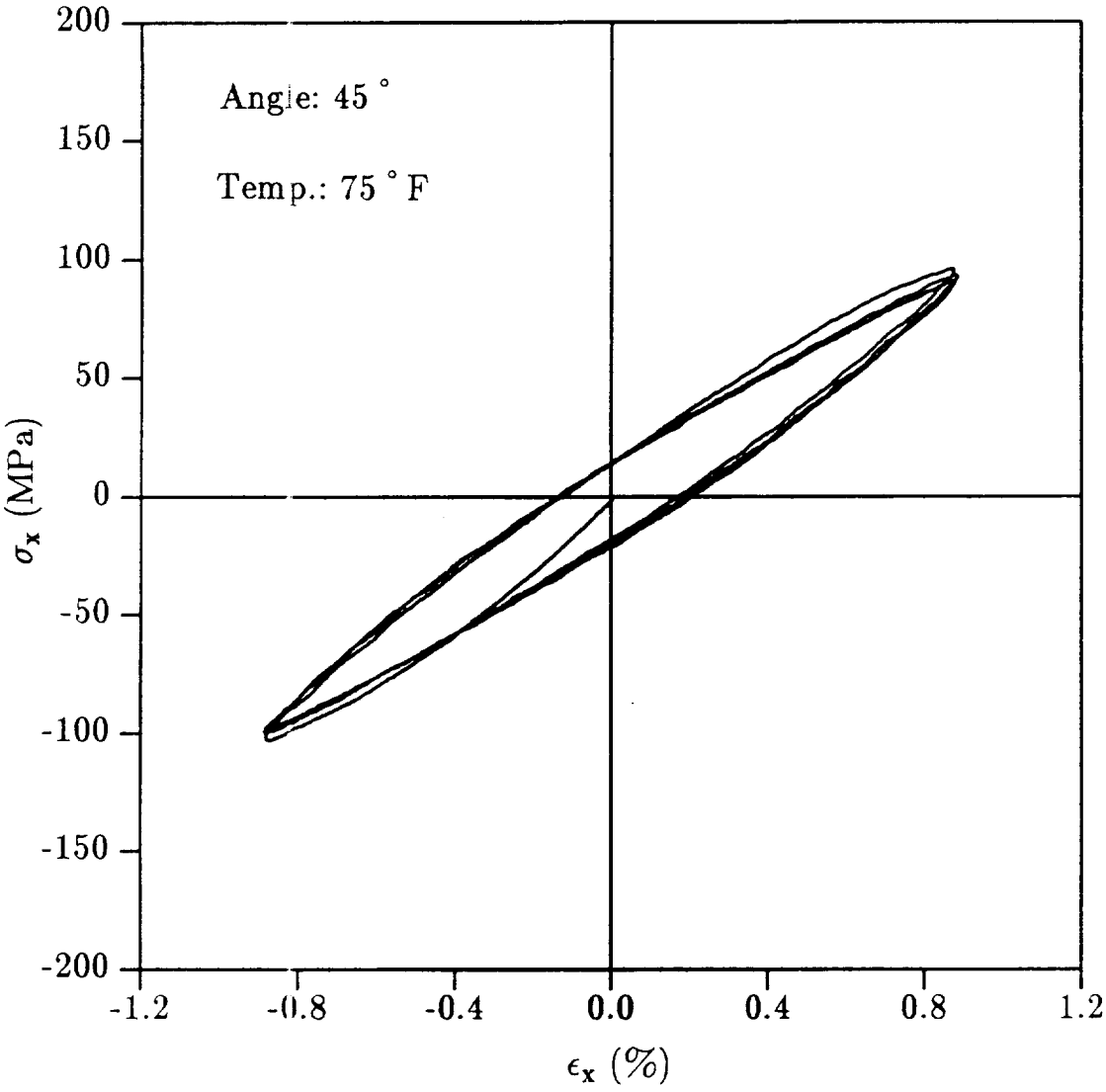

Fig. 4. Stress-strain curve for 45° off-axis specimen of AS4/APC-2 composite at 75°F for first 6 reversals.

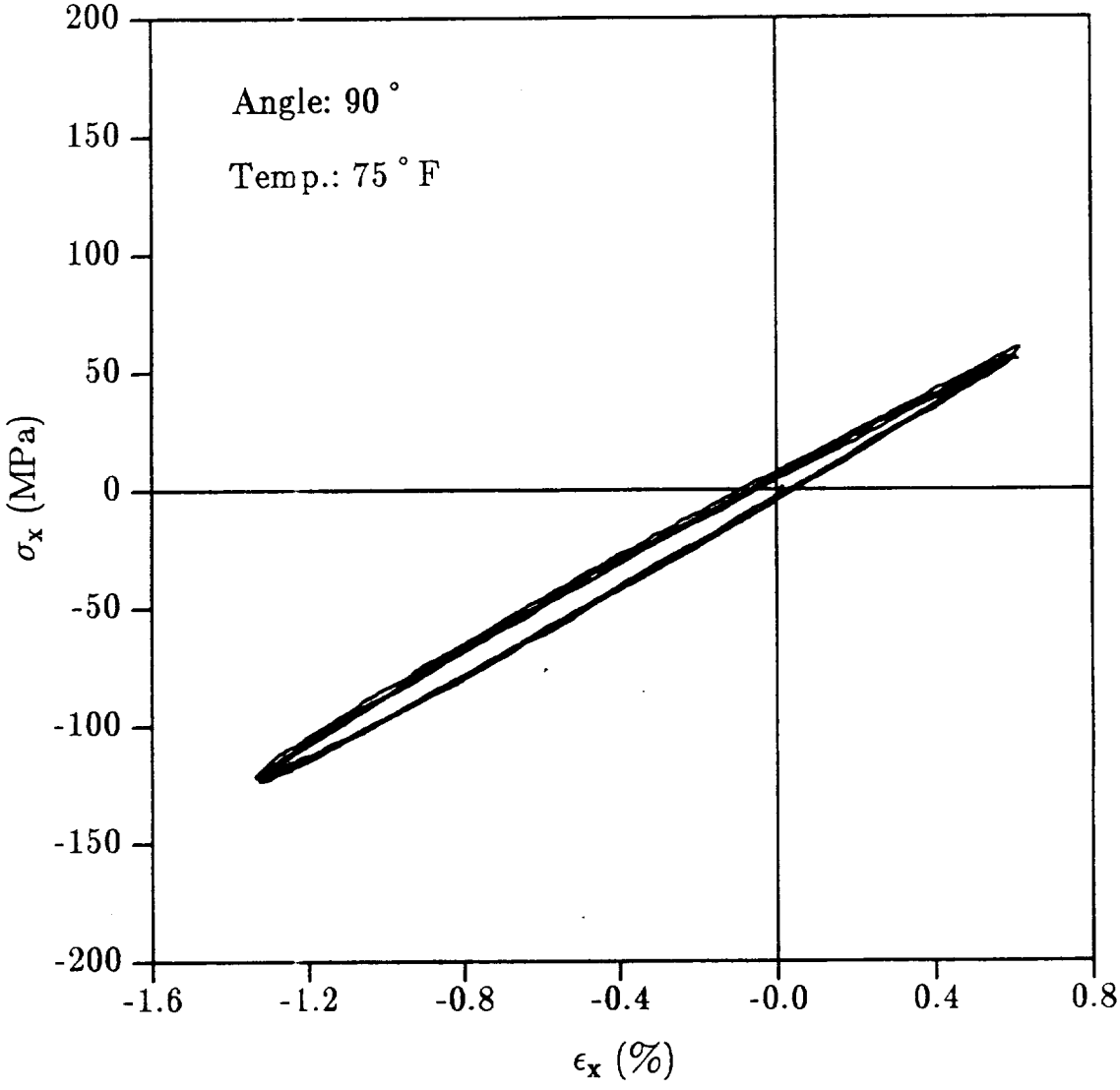

Fig. 5. Stress-strain curve for 90° off-axis specimen of AS4/APC-2 composite at 75°F for first 8 reversals.

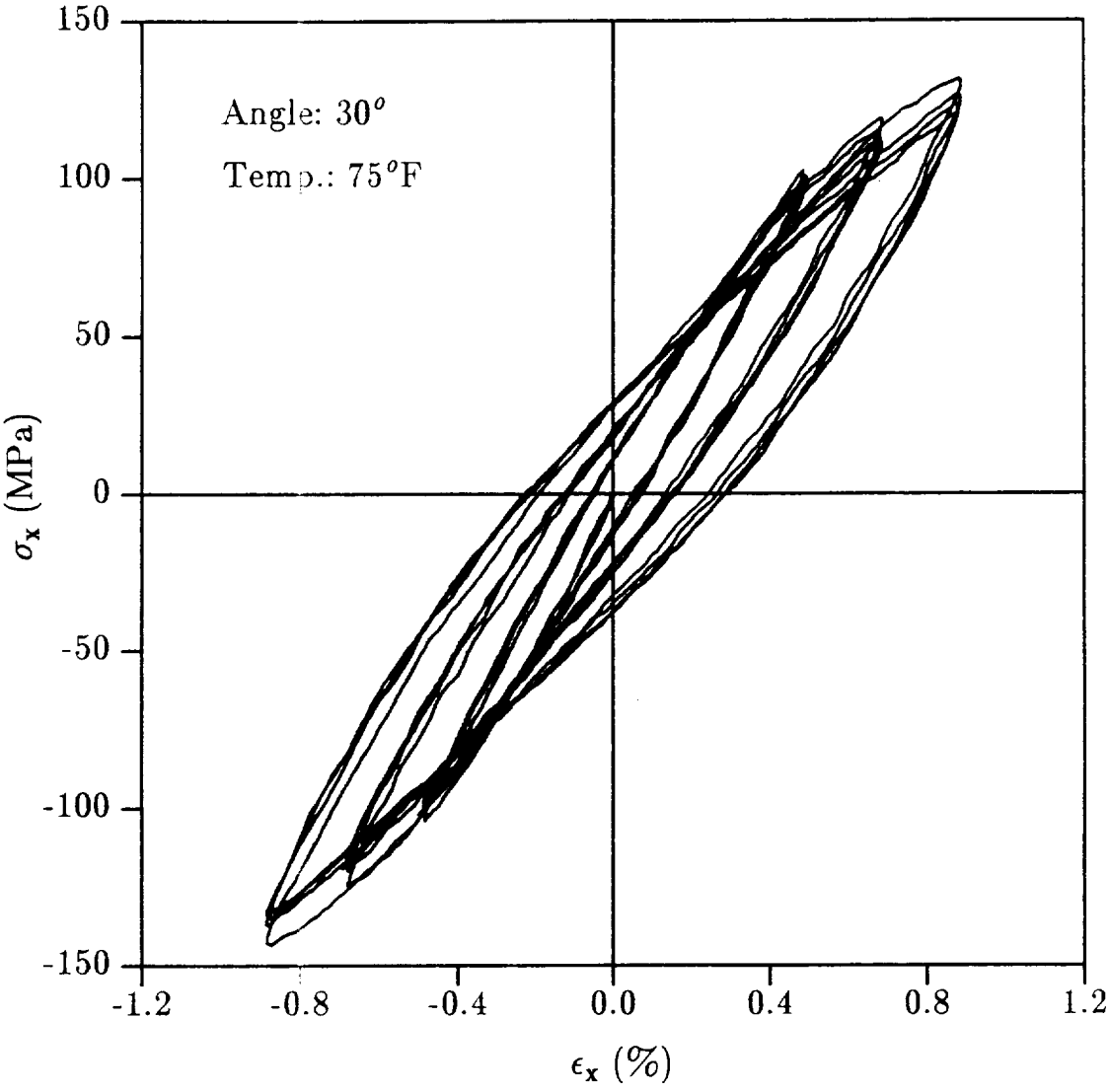

Fig. 6. Stress-strain curves for 30° off-axis specimen of AS4/APC-2 composite at 75°F.

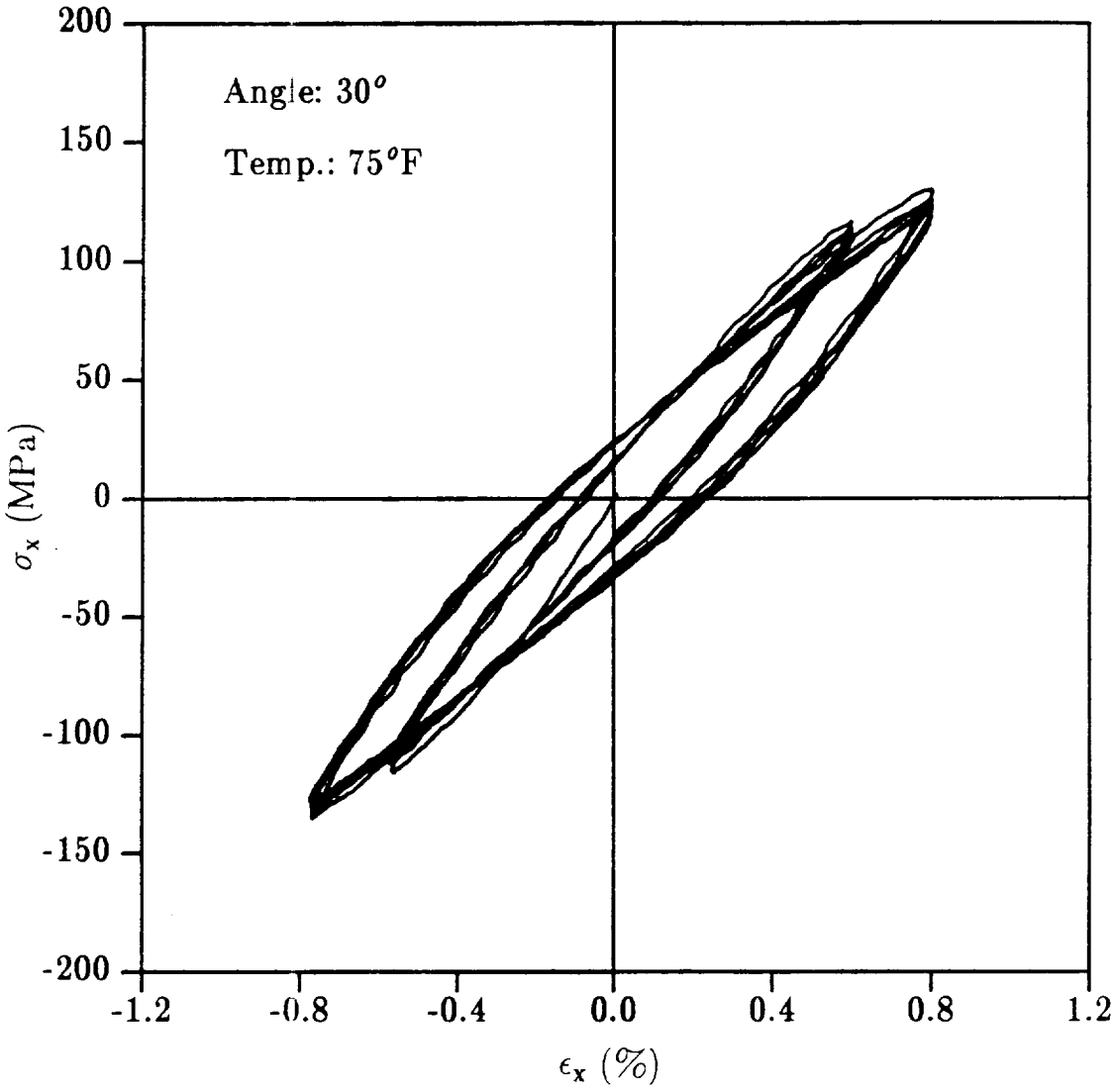

Fig. 7. Stress-strain curve for 30° off-axis specimen of AS4/APC-2 composite with increasing strain range at 75°F.

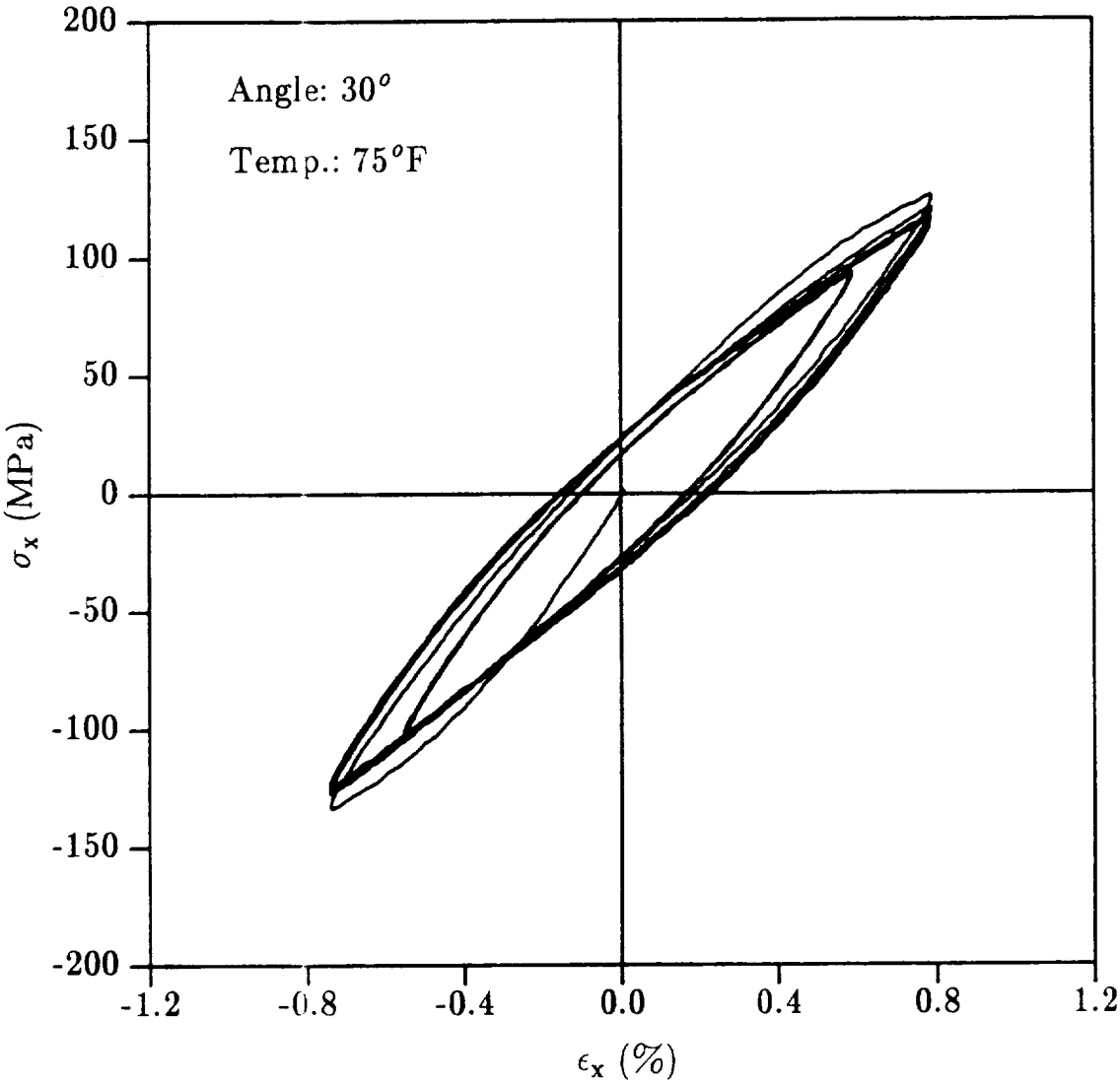

Fig. 8. Stress-strain curve for 30° off-axis specimen of AS4/APC-2 composite with decreasing strain range at 75°F.

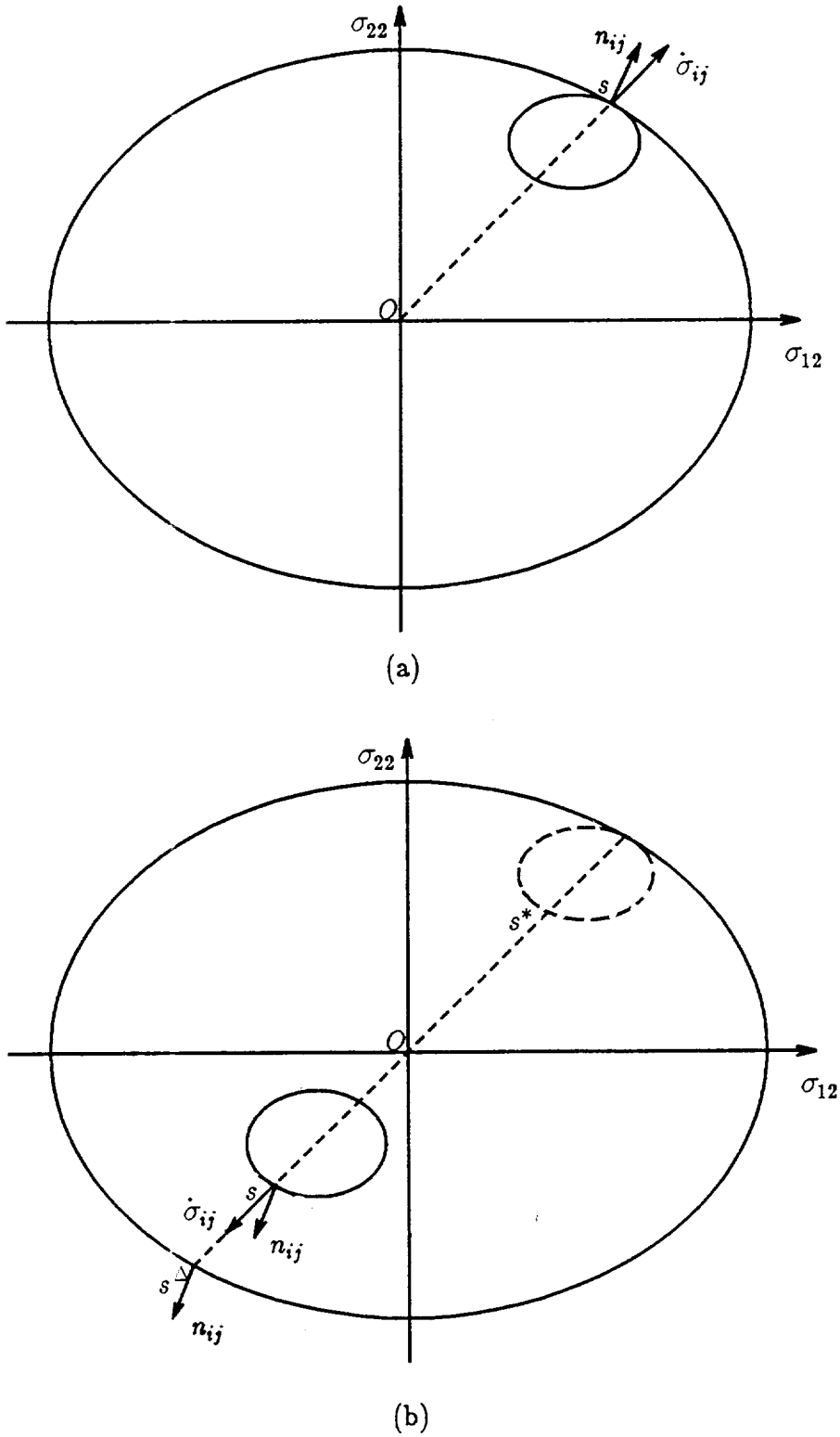

Fig. 9. Schematic representation of the yield surface and the memory surface. (a). for virgin deformation process. (b). for non-virgin deformation process.

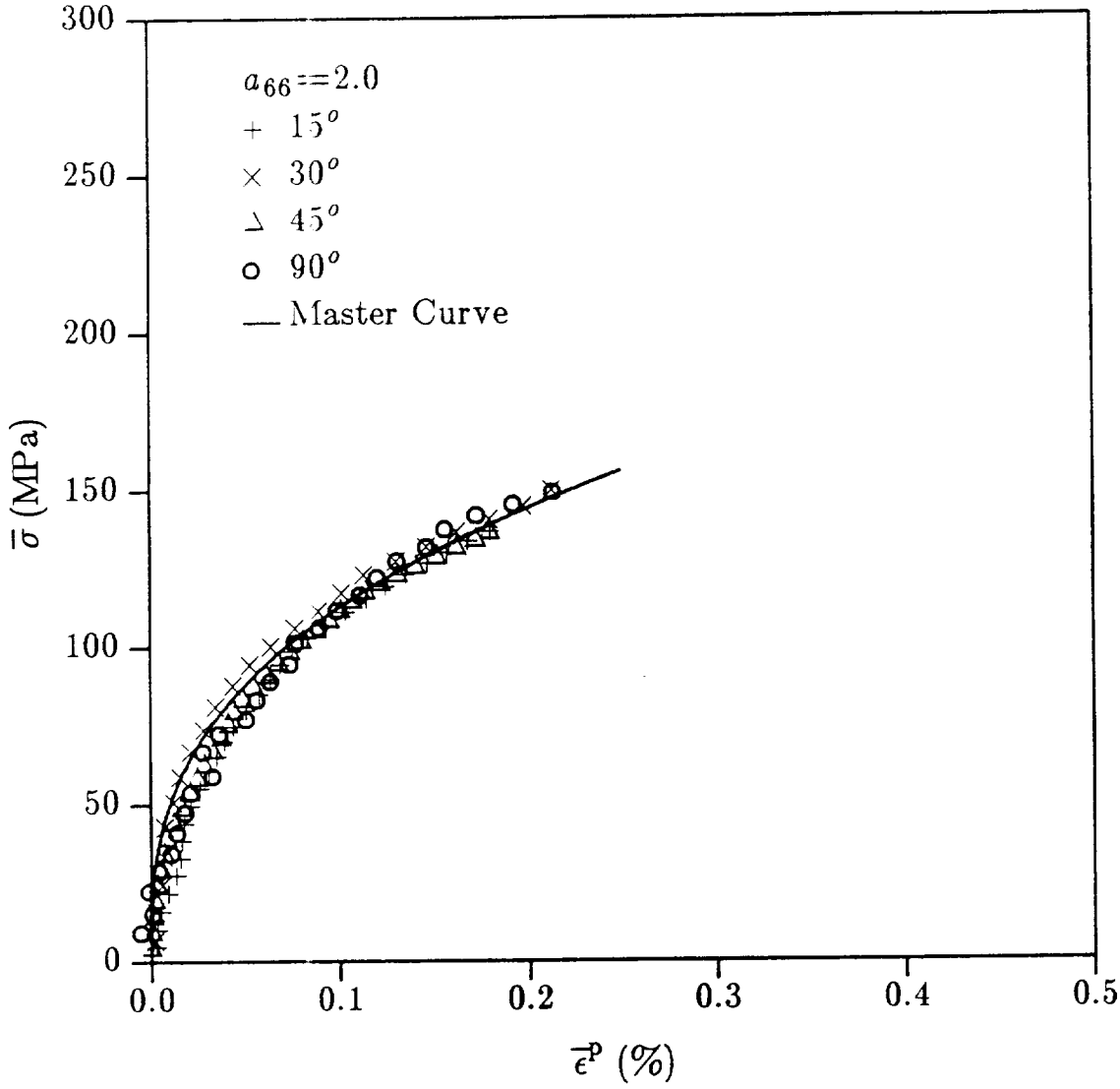

Fig. 10. Experimental data of $\bar{\sigma}$ vs. $\bar{\epsilon}^p$ for initial loading and fitted curve by the power law $\bar{\epsilon}^p = A(\bar{\sigma})^n$.

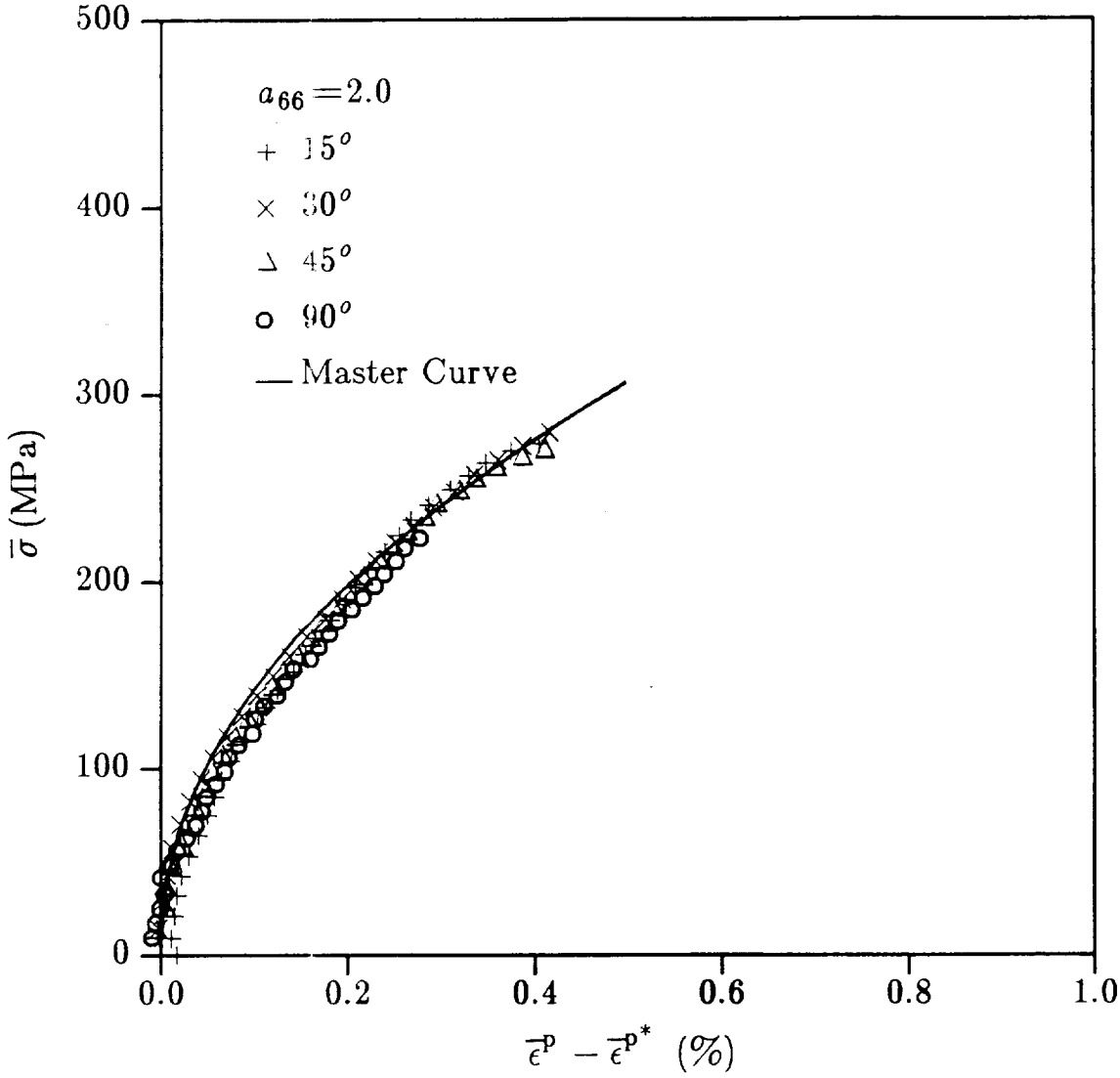

Fig. 11. Experimental data of $\bar{\sigma}$ vs. $(\bar{\epsilon}^p - \bar{\epsilon}^{p*})$ for first reversal and fitted curve by the power law $(\bar{\epsilon}^p - \bar{\epsilon}^{p*}) = A(\bar{\sigma})^n$; $q_{max} = 148$ MPa.

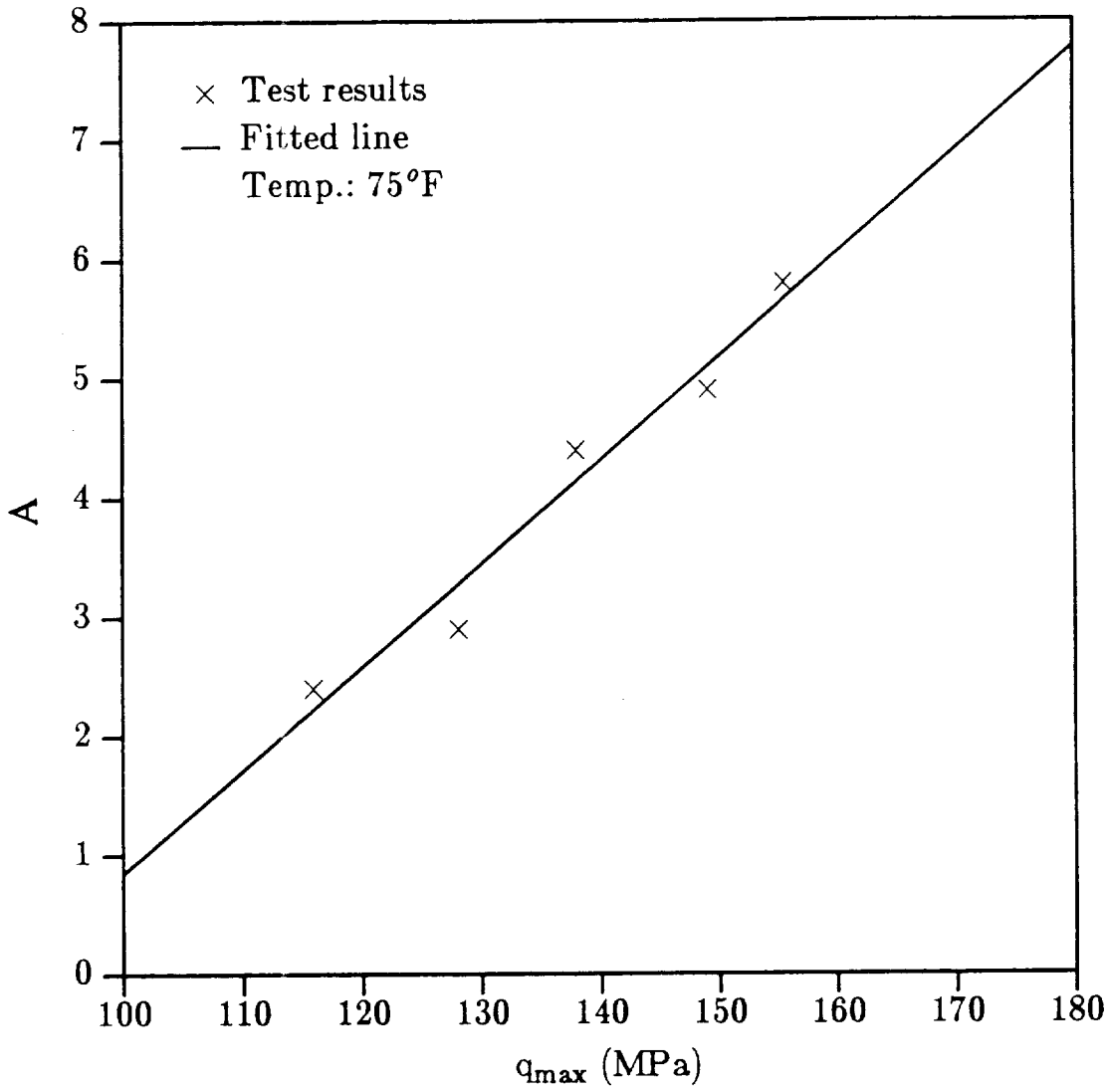

Fig. 12. Effect of Loading range on hardening property.

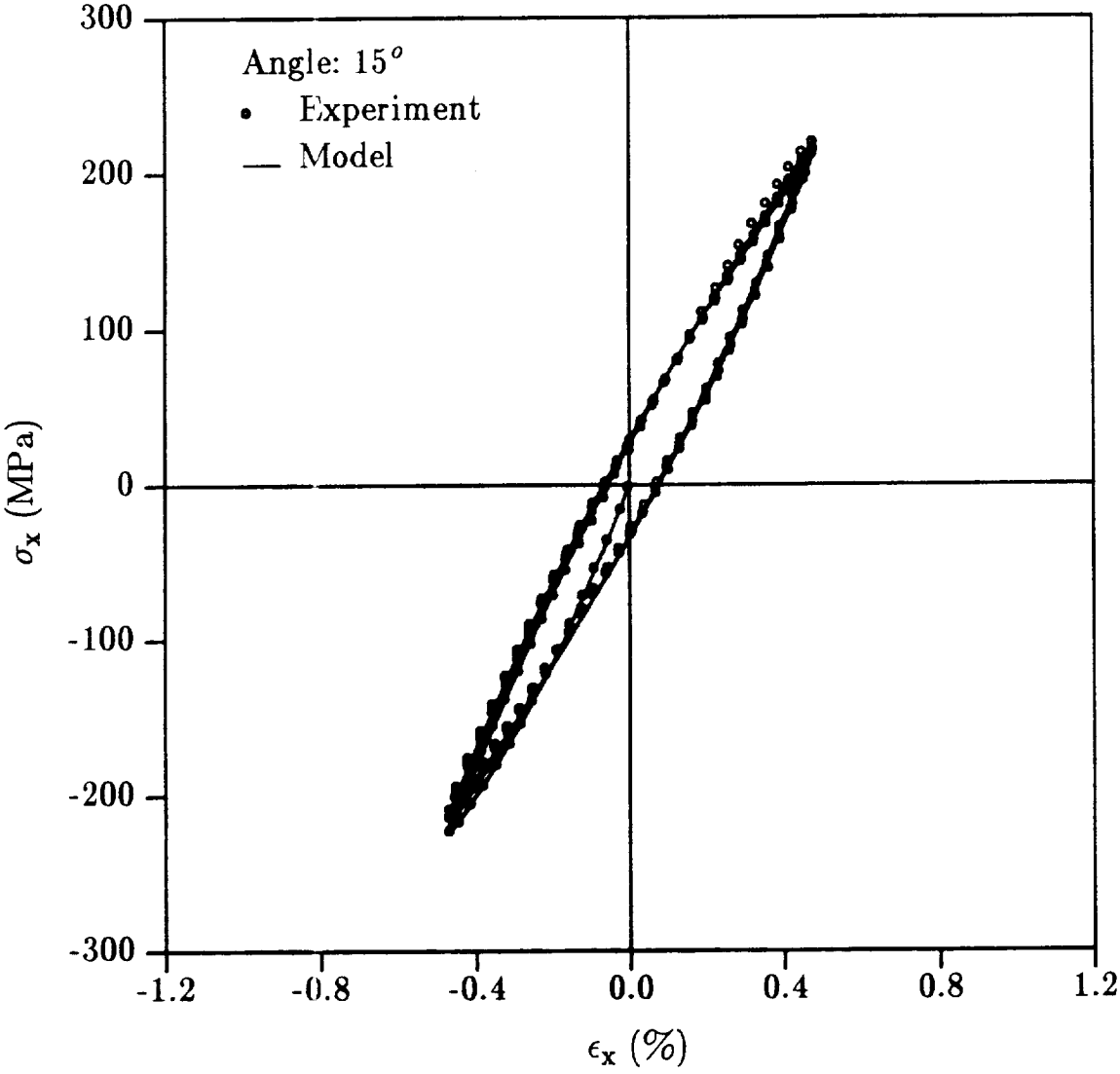

Fig. 13. Comparison of experimental result with model simulation of stress-strain curve for 15 ° off-axis specimen of AS4/APC-2 composite at 75 ° F.

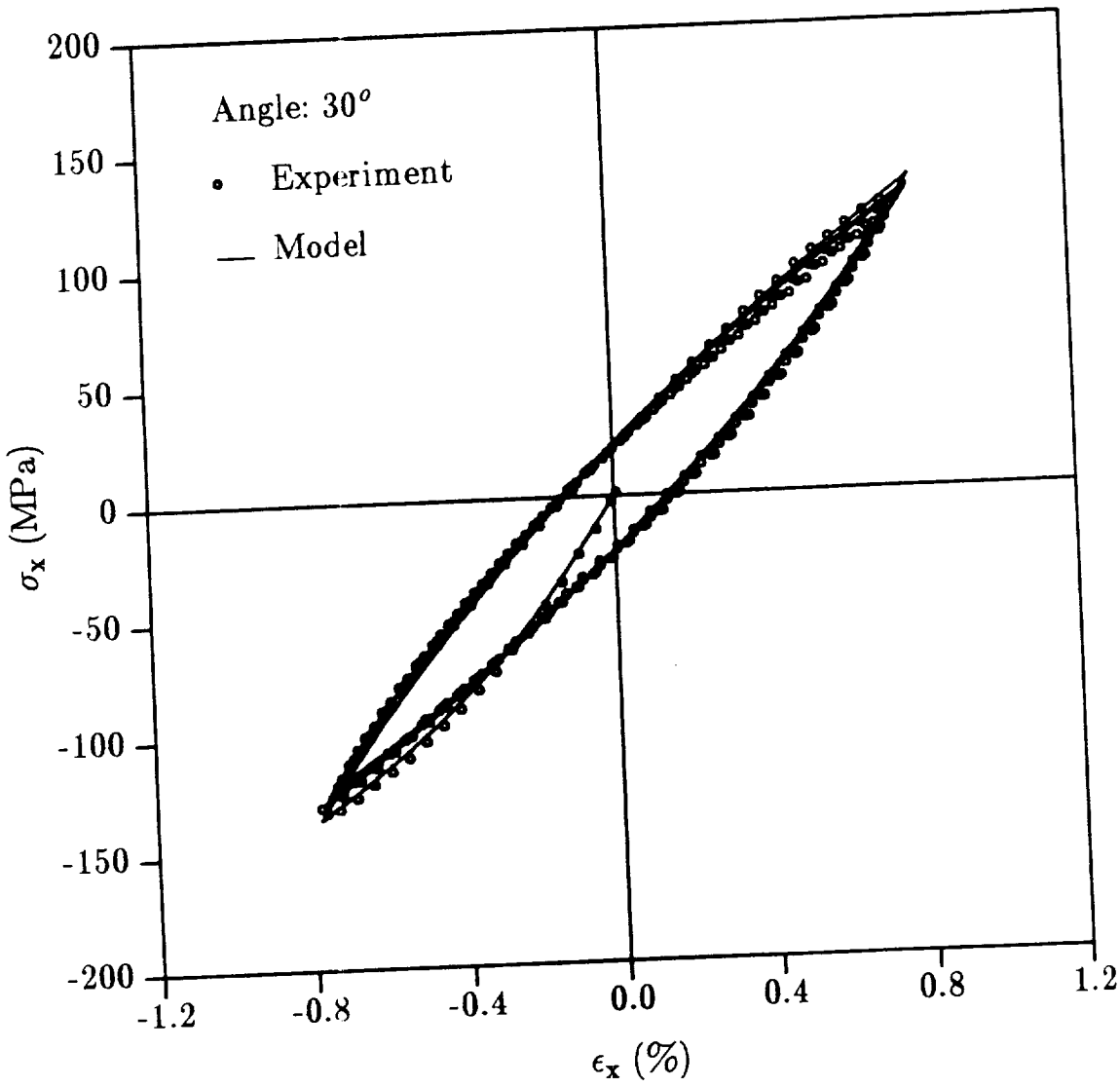

Fig. 14. Comparison of experimental result with model simulation of stress-strain curve for 30 ° off-axis specimen of AS4/APC-2 composite at 75 ° F.

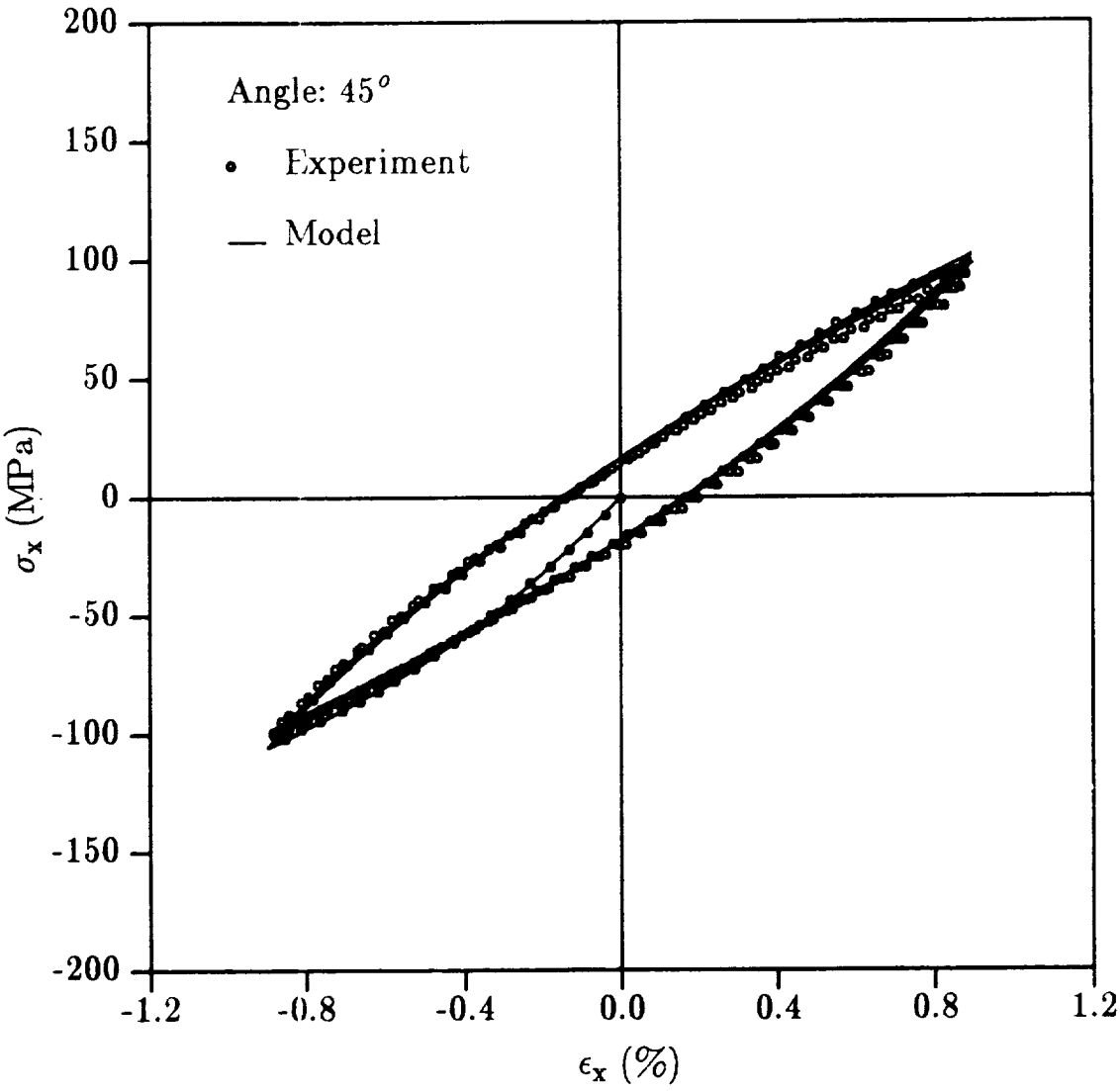

Fig. 15. Comparison of experimental result with model simulation of stress-strain curve for 45° off-axis specimen of AS4/APC-2 composite at 75° F.

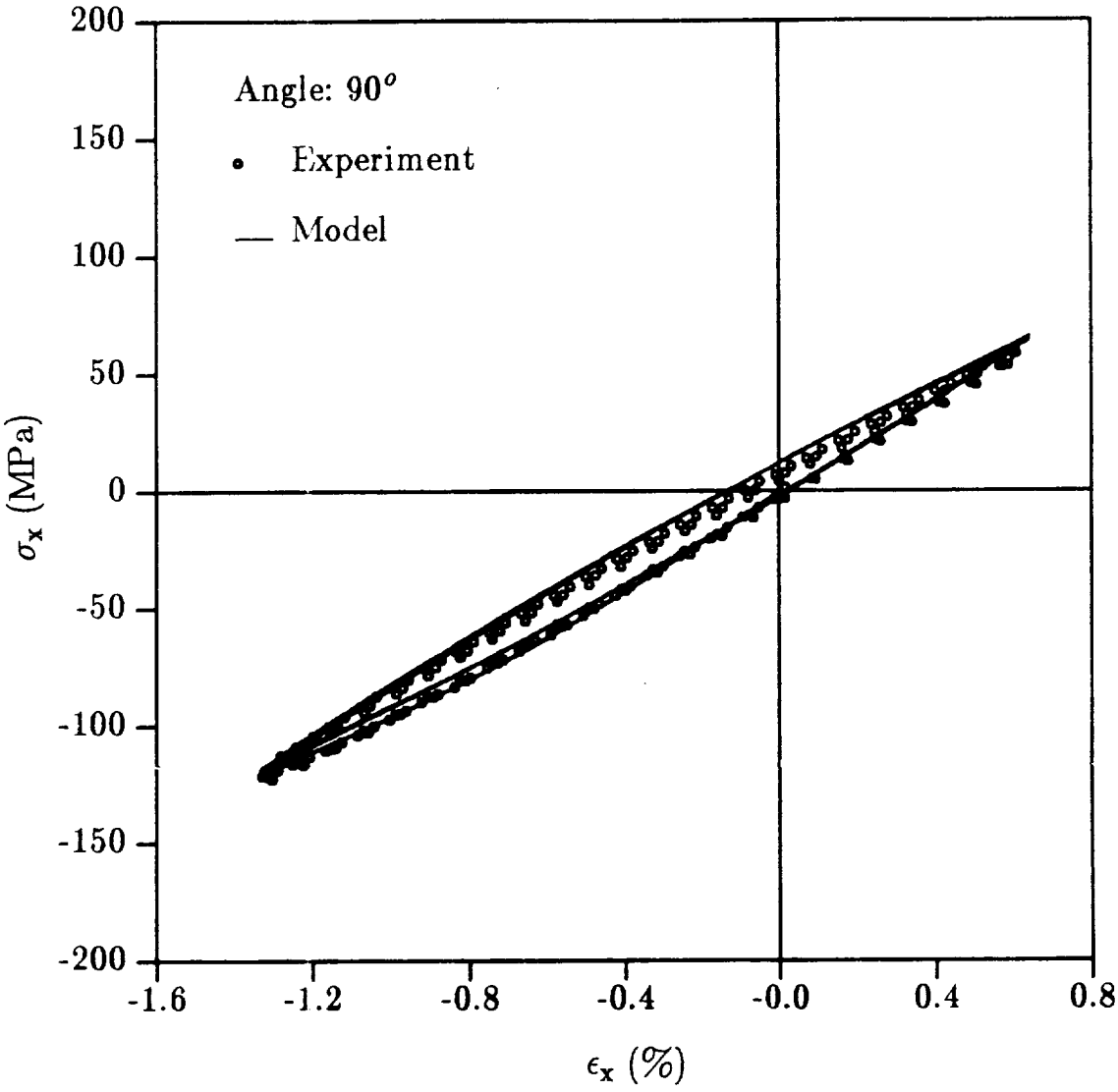

Fig. 16. Comparison of experimental result with model simulation of stress-strain curve for 90° off-axis specimen of AS4/APC-2 composite at 75° F.

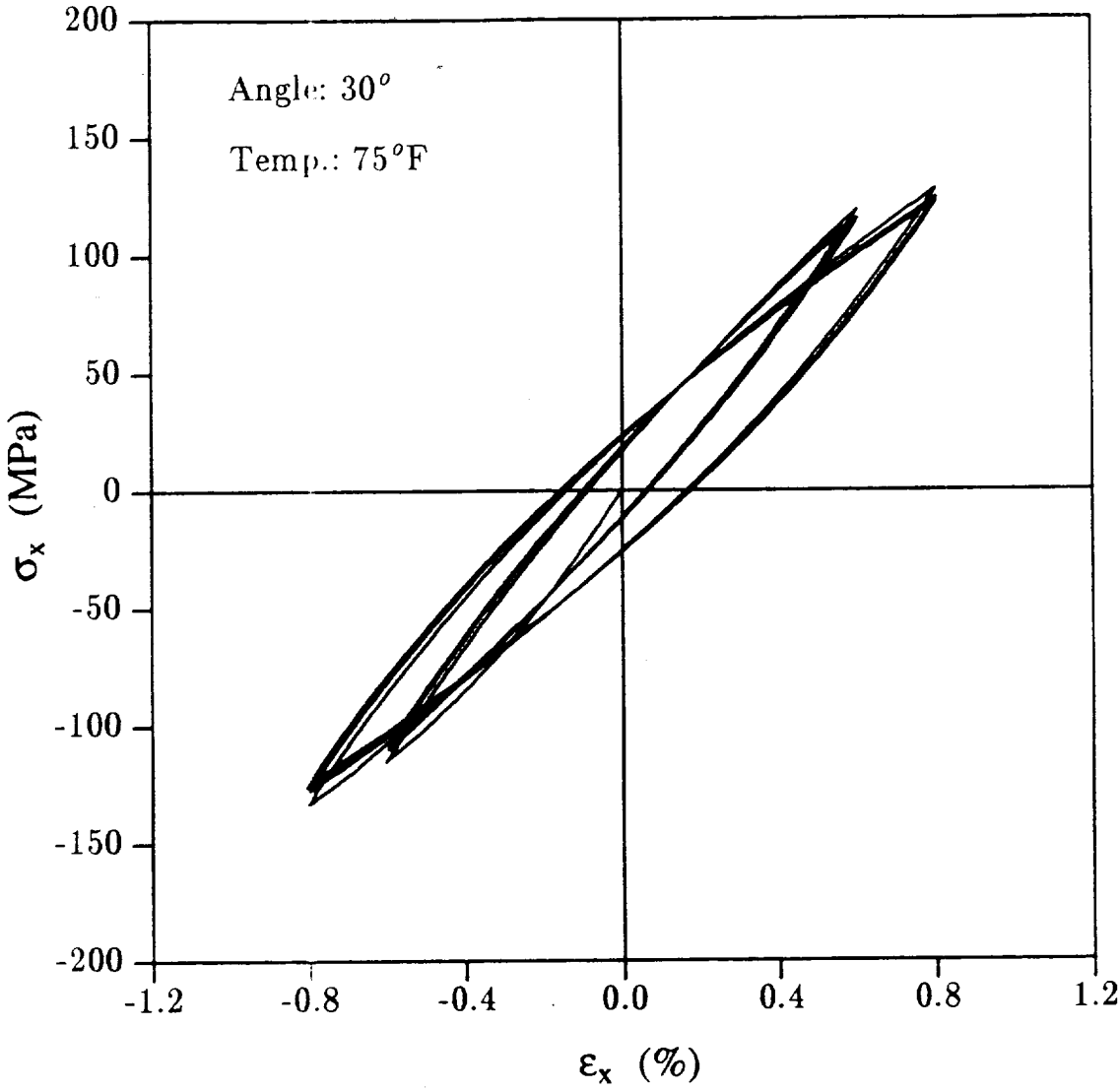

Fig. 17. Model simulation of stress-strain curve for 30° off-axis specimen of AS4/APC-2 composite with increasing strain range at 75° F.

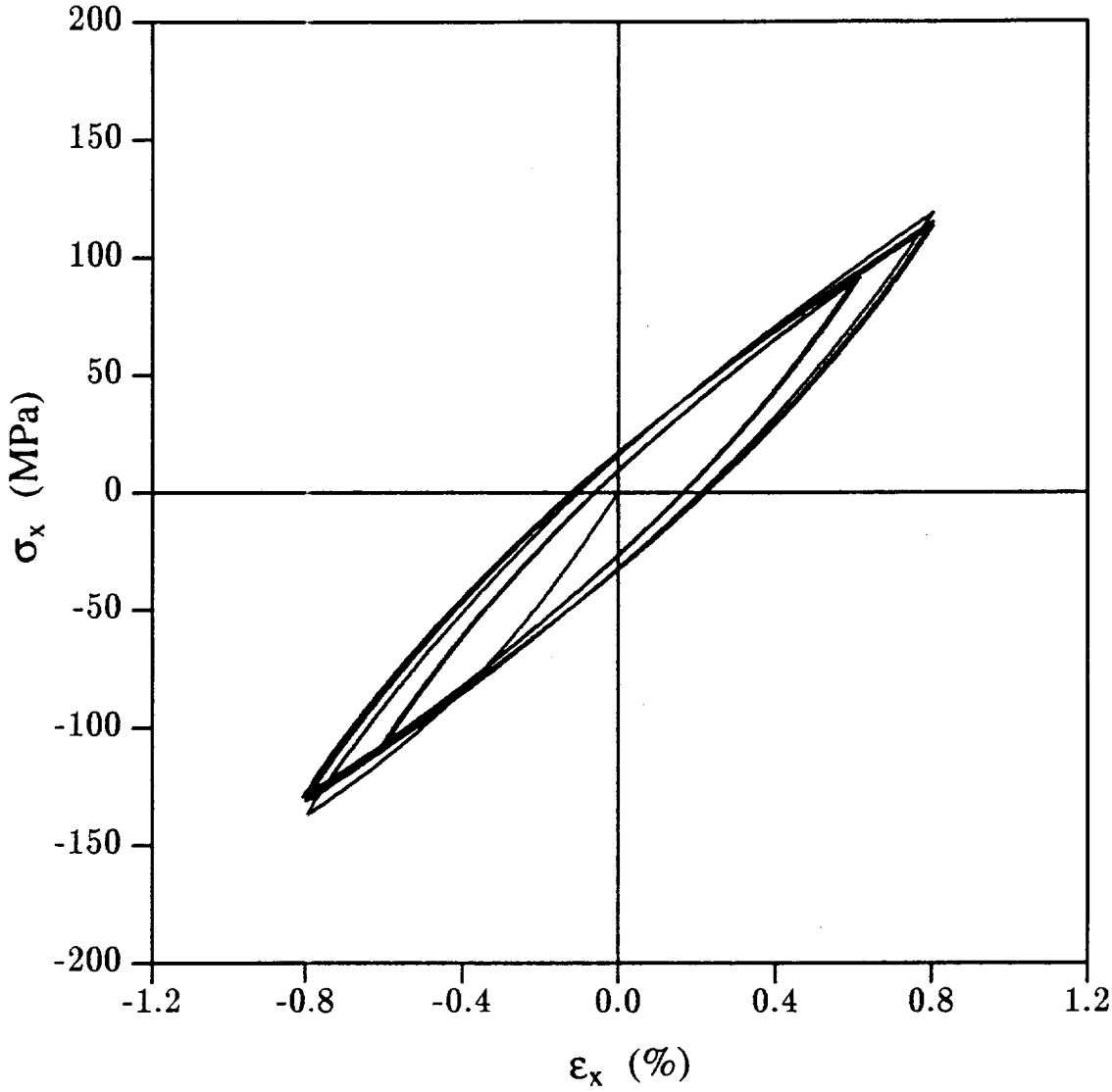

Fig. 18. Model simulation of stress-strain curve for 30° off-axis specimen of AS4/APC-2 composite with decreasing strain range at 75° F.